

Article

# Liquiritigenin attenuates myocardial ischemia-reperfusion injury by activating the Nrf2/HO-1 pathway

Huiyu Jia<sup>1,†</sup>, Ting Wang<sup>2,†</sup>, Min Si<sup>1,†</sup>, Zheng Ma<sup>1</sup>, Shengyong Luo<sup>1,\*</sup><sup>1</sup> Anhui Medical College (Anhui Academy of Medical Sciences), Hefei 230061, China<sup>2</sup> School of Basic Medicine, Anhui Medical University, Hefei 230031, China\* **Corresponding author:** Shengyong Luo, [lsy770728@126.com](mailto:lsy770728@126.com)

† These authors contributed equally.

## CITATION

Jia H, Wang T, Si M, et al.  
Liquiritigenin attenuates myocardial ischemia-reperfusion injury by activating the Nrf2/HO-1 pathway.  
*Journal of Biological Regulators and Homeostatic Agents*. 2025; 39(2): 3397.  
<https://doi.org/10.54517/jbrha3397>

## ARTICLE INFO

Received: 6 March 2025

Accepted: 20 March 2025

Available online: 31 March 2025

## COPYRIGHT



Copyright © 2025 by author(s).  
*Journal of Biological Regulators and Homeostatic Agents* is published by Asia Pacific Academy of Science Pte. Ltd. This work is licensed under the Creative Commons Attribution (CC BY) license.  
<https://creativecommons.org/licenses/by/4.0/>

**Abstract: Background:** The Nrf2/HO-1 signaling pathway is a critical antioxidative stress and cytoprotective pathway, and oxidative stress plays a significant role in myocardial ischemia-reperfusion injury (MIRI). Liquiritigenin, a flavonoid compound derived from licorice, is hypothesized to alleviate MIRI, though its specific mechanism remains unclear. **Methods:** Following a 15-min pretreatment with liquiritigenin, animals underwent myocardial ischemia-reperfusion injury induction comprising 30-min coronary occlusion and 2-h reperfusion. Continuous cardiac monitoring incorporated both electrocardiography (ECG) and ventricular pressure dynamics, specifically tracking systolic pressure (LVSP), end-diastolic pressure (LVEDP), and ventricular contractility indices ( $\pm dp/dt_{max}$ ). Post-experimental biospecimen analysis included: Myocardial injury evaluation: Serum quantification of lactate dehydrogenase and CK-MB isoenzyme levels. Redox status assessment: Measurement of antioxidant enzyme activities (SOD, GSH) and lipid peroxidation biomarker MDA concentration. Histopathological damage: Evaluated via hematoxylin-eosin (HE) staining. Apoptosis: Detected by TUNEL assay. Protein expression: Western blot analysis of Nrf2/HO-1 pathway components (Nrf2, Keap1, HO-1). **Conclusion:** Liquiritigenin exerts cardioprotective effects against MIRI by activating the Nrf2/HO-1 signaling pathway, thereby attenuating post-reperfusion oxidative stress. This study elucidates the central role of Nrf2/HO-1 pathway interactions in MIRI and identifies liquiritigenin as a potential therapeutic candidate for targeting this pathway.

**Keywords:** myocardial ischemia-reperfusion injury; Nrf2/HO-1; oxidative stress

## 1. Introduction

Myocardial ischemia-reperfusion injury (MIRI) is a common complication during reperfusion therapy for acute myocardial infarction. Its pathological mechanisms are closely associated with oxidative stress bursts [1], inflammatory cascades [2], and cellular apoptosis [3]. While reperfusion therapy can rescue heart tissue deprived of oxygen, it comes with a double-edged sword: the excessive generation of reactive oxygen species (ROS). This surge in ROS triggers a cascade of damaging effects, including the breakdown of cell membranes through lipid peroxidation, disruption of mitochondrial function, and ultimately, the death of heart muscle cells. These unintended consequences severely undermine the therapeutic benefits, leaving much to be desired in terms of clinical outcomes [4]. Consequently, targeted regulation of oxidative stress responses has emerged as a pivotal strategy for mitigating MIRI.

The nuclear factor erythroid 2-related factor 2 (Nrf2) and its downstream effector,

heme oxygenase-1 (HO-1), function as a master regulatory axis that bucks oxidative stress. They work in tandem to oversee the cellular antioxidant defenses. This transcriptional system mediates phase II detoxification through upregulating enzymatic scavengers including superoxide dismutase and glutathione peroxidase, thereby neutralizing ROS and preserving intracellular redox equilibrium. Research shows that Nrf2/HO-1 pathway activation significantly reduces myocardial damage in MIRI [5]; however, its mechanistic role in natural compound-based interventions remains incompletely elucidated. Liquiritigenin, a flavonoid isolated from the traditional Chinese herb *Glycyrrhiza uralensis*, exhibits anti-inflammatory, antioxidant, and cardioprotective properties [6]. Preliminary studies suggest its potential to exert myocardial protection via oxidative stress pathway modulation, yet further exploration is needed for its specific regulatory impacts on the Nrf2/HO-1 axis and the molecular mechanisms involved in MIRI.

This research seeks to clarify how liquiritigenin protects the heart from ischemia-reperfusion damage (MIRI) through the Nrf2/HO-1 signaling pathway. Using a validated rat MIRI model, we comprehensively assessed liquiritigenin's effects on cardiac function, oxidative damage, and apoptosis through hemodynamic analysis, oxidative stress biomarker quantification, and molecular techniques. Additionally, its regulatory effects on Nrf2 nuclear translocation, Keap1 interaction, and HO-1 expression were investigated. Our findings offer the first experimental evidence that liquiritigenin mitigates oxidative stress by activating this pathway, laying a foundation for developing novel therapeutics targeting Nrf2/HO-1 for myocardial protection.

## **2. Materials and methods**

### **2.1. Materials**

Liquiritigenin CAS: 578-86-9, 98.14% pure, was sourced from Shanghai McLean Biochemical Technology Co., LTD. (Shanghai, China). Diltiazem hydrochloride tablets are manufactured by Shanghai Xinyi Wanxiang Pharmaceutical Co., LTD. (Shanghai, China). The One-Step TUNEL Apoptosis Detection Kit (red fluorescence) was purchased from Beyotime Biotechnology (Shanghai, China). Primary antibodies against Nrf2 (rabbit polyclonal, #AF0639), HO-1 (mouse monoclonal, #AF0243), Keap1 (rabbit monoclonal, #AF0821), and  $\beta$ -actin (mouse monoclonal, #AF0003) were obtained from Wuhan Sanying Biotechnology (Wuhan, China).

### **2.2. Surgical procedures**

Rats were given water after a 12-h fast prior to surgery, weighed, and induced anesthesia by intraperitoneal injection of 5% chloral hydrate at a dose of 6 mL/kg. After anesthesia, rats were positioned supine, with the neck and precordial area prepared for skin disinfection. Tracheotomy was performed, and rats were connected to a small animal respirator (tidal volume 11 mL/kg, respiratory rate 70 breaths/min) to maintain normal respiration. After stable breathing was achieved, rats were connected to an electrocardiograph for recording leads II of the electrocardiogram. To gain entry into the chest cavity, a thoracotomy was carefully executed between the third and fourth ribs on the left side. The pericardium was then incised, providing a

clear, unobstructed view of the heart. The left anterior descending coronary artery was identified, situated between the pulmonary artery cone and the left atrial appendage. Using a 7/0 suture, the artery was ligated at a point just below the appendage's root, approximately 2–4 mm from the pulmonary artery cone. Following a 30-min period of occlusion, the ligature was released, allowing for reperfusion to occur over the next 120 min. Successful modeling criteria: after ligation, part of the left ventricular myocardium appeared pale or cyanotic, and the ECG showed significant ST segment elevation or elevated T waves, indicating successful ischemia; after releasing the ligature, the color of the ischemic area in the left ventricle turned red, and the ST segment returned to half of the previous elevation, indicating successful reperfusion.

### **2.3. Grouping, and treatment**

A total of 80 SPF SD rats with a body mass of 250–300 g, half male and half female, were selected and fed in cages for 7 days. They were split into six groups via the random number table approach. These groups included the sham operation group (referred to as the sham group), the model group (the MIRI group), the liquiritigenin high-dose group (LIQ-H, at a dosage of 30 mg/kg/day), the liquiritigenin medium-dose group (LIQ-M, with a 20 mg/kg/day dosage), the liquiritigenin low-dose group (LIQ-D, having a 10 mg/kg/day dose), and the diltiazem group (DIL, with a 10 mg/kg/day dose). Each group consisted of 10 rats; the sham and MIRI groups received identical 0.9% sodium chloride solution volumes via intragastric administration over 3 days. The Sham group was threaded into the coronary artery without ligation. Myocardial ischemia for 30 min and reperfusion for 120 min were performed in the other groups. Another 20 SD rats were selected for reserve. In cases where the intended number of animals per experimental group fell short due to challenges such as adaptive feeding, drug administration, or issues during the modeling phase, the final count was adjusted to 10 animals per group.

### **2.4. Electrocardiogram (ECG) recording**

Rats were anesthetized via intraperitoneal pentobarbital sodium (40 mg/kg) and placed in a supine position. The electrodes for standard limb lead II were attached to the BL-420S Biological Signal Acquisition and Analysis System (Chengdu TME Technology Co., Ltd., China). Continuous ECG signals were captured at a sampling rate of 1 kHz for 10 min following modeling to assess ST-segment elevation, T-wave inversion, and the occurrence of arrhythmias. Data were analyzed using system-integrated software (TaiMeng Analysis Suite v5.0) with baseline correction and noise filtering (50 Hz notch filter).

### **2.5. Hemodynamic parameter assessment**

A polyethylene catheter was retrogradely advanced from the right common carotid artery into the left ventricle. The BL-420S system was used to continuously monitor hemodynamic indices, namely left ventricular systolic pressure (LVSP), left ventricular end-diastolic pressure (LVEDP), and the maximum rates of pressure increase and decrease ( $\pm dp/dt_{max}$ ). Signals were digitized at 500 Hz, and data were averaged over 30-s intervals during stable hemodynamic phases (pre-ischemia,

ischemia, and reperfusion).

## **2.6. TTC**

Collect heart tissue samples and rapidly freeze them at  $-20\text{ }^{\circ}\text{C}$  for 30 min. Slice the tissue into 1 mm-thick sections and transfer them into a culture dish containing TTC staining solution. Incubate the dish in a  $37\text{ }^{\circ}\text{C}$  thermostat-controlled incubator protected from light for 30 min of staining, periodically removing the container to gently agitate the sections during this process. After staining, carefully rinse off excess TTC staining solution with PBS, then photograph the samples.

## **2.7. Histopathological examination**

Hearts were excised and perfused with ice-cold PBS. Heart tissue samples obtained from the area surrounding the left anterior descending coronary artery were preserved using a 4% neutral-buffered paraformaldehyde solution for a full day. Afterward, they were dehydrated through a series of ethanol concentrations, embedded in paraffin wax, and sliced into ultra-thin sections measuring 4 micrometers. To evaluate the tissue's structural condition—including disruptions in myofibril arrangement, fluid buildup in the interstitial spaces, and signs of inflammation—the sections were treated with hematoxylin and eosin (H.E.) staining.

## **2.8. Myocardial injury biomarker quantification**

Blood samples were collected via the abdominal aorta and centrifuged ( $3000 \times g$ , 15 min) to isolate serum. Serum concentrations of LDH and CK-MB enzymes were quantified using an automatic biochemical analyzer, while cardiac troponin T (cTnT) was measured with a high-sensitivity ELISA kit (CSB-E17300r, Cusabio Technology, China) according to the manufacturer's instructions. The absorbance of samples at 450 nm was detected using the Thermo Scientific™ Multiskan™ FC microplate reader.

## **2.9. Oxidative stress and antioxidant activity assays**

The detection methods for SOD, GSH, and MDA are identical, employing an enzyme-linked immunosorbent assay kit. Take out the required strip plates from the aluminum foil bag after it has been equilibrated at room temperature for 20 min. Set up standard sample wells and test sample wells. Add 50  $\mu\text{L}$  of standard samples with different concentrations to each of the standard sample wells. Put 50  $\mu\text{L}$  of the sample to be tested into the test sample wells; leave the blank well empty. Except for the blank well, add 100  $\mu\text{L}$  of the detection antibody labeled with horseradish peroxidase (HRP) to each of the standard sample wells and test sample wells. Seal the reaction wells with a plate-sealing film and incubate them in a  $37\text{ }^{\circ}\text{C}$  water bath or incubator for 60 min. Then, use a plate washer to wash the plates. Add 50  $\mu\text{L}$  each of substrate A and substrate B to every well, and incubate in the dark at  $37\text{ }^{\circ}\text{C}$  for 15 min. Next, add 50  $\mu\text{L}$  of the stop solution to each well. Within 15 min, measure the OD value of each well at a wavelength of 450 nm.

## **2.10. TUNEL apoptosis assay**

Cardiac tissue slices were deparaffinized, rehydrated, and incubated with a 20

$\mu\text{g/mL}$  DNase-free proteinase K solution at 37 °C for 20 min, subsequently undergoing three washes with phosphate-buffered saline (PBS; 5 min each). A TUNEL detection solution was formulated by combining TdT enzyme and fluorescein-labeled dUTP, completely vortexed, and shielded from light. Following two supplementary PBS washes, 50  $\mu\text{L}$  of the TUNEL reaction mixture was administered to thoroughly encompass the tissue sections, which were then incubated in a dark, humidified chamber at 37 °C for one hour. Following incubation, slices were rinsed thrice with PBS (5 min each), counterstained with DAPI (1  $\mu\text{g/mL}$ ) for 5 min in light-protected conditions, and subsequently washed three times with PBS. Slides were affixed using an anti-fade mounting media (ProLong Gold, Thermo Fisher) and examined under a fluorescence microscope (excitation/emission wavelengths: TUNEL 550/570 nm, DAPI 358/461 nm). The apoptotic index was calculated as the percentage of TUNEL-positive nuclei relative to total nuclei (TUNEL-positive nuclei/total nuclei  $\times$  100%).

### **2.11. Western blot analysis of Nrf2/HO-1 pathway**

On ice, myocardial tissue samples (30 mg) were homogenized in 1.0 mL of RIPA lysis buffer with 1  $\mu\text{M}$  PMSF until fully lysed. Subsequently, the lysate was centrifuged at  $1200 \times g$  for 5 min at 4 °C. Discard the supernatant and resuspend the pellet in 150  $\mu\text{L}$  of lysis solution with 1% PMSF, followed by a 30-min incubation on ice with vortex mixing every 10 min. After three rounds of mixing, the lysate was spun down at  $15,000 \times g$  for a quarter of an hour at 4 °C. The resulting supernatant, which was the total protein extract, was then retrieved. To ensure consistent loading, the protein concentration was determined via a BCA assay. Under denaturing conditions, proteins were separated through SDS-PAGE and then transferred to PVDF membranes at a current of 250 mA for an hour. The membranes were incubated with 5% skim milk for two hours at room temperature. After that, they were incubated overnight at 4 °C with primary antibodies (Nrf2, HO-1, Keap1). After being washed three times with TBST, the membranes were incubated with HRP-conjugated secondary antibodies at 37 °C for an hour. Subsequently, they were washed three times with TBST and distilled water, and detection was carried out using an ECL detection kit. After exposure, the intensities of the bands were assessed via a gel imaging method.

### **2.12. Replication of the cell oxygen-glucose deprivation and reoxygenation model**

H9c2 myocardial cells were grown until they reached the desired confluency. The initial culture medium was carefully removed, and the cells were rinsed twice with phosphate-buffered saline (PBS). Subsequently, Earle's balanced salt solution, devoid of glucose, was introduced. The cells were then transferred to a hypoxic culture chamber, maintained at 37 °C, with an atmosphere composed of 95% nitrogen and 5% carbon dioxide. After 3 h of glucose and oxygen deprivation, reoxygenation and glucose replenishment were achieved, with a reoxygenation and glucose replenishment time of 12 h. Simulated reperfusion injury was performed, and cell growth in each group was observed under a microscope.

### **2.13. Cell group intervention**

H9c2 cells were cultured to a certain concentration, seeded into 6-well plates, and divided into several groups: normal group (control group), oxygen-glucose deprivation/reoxygenation group (OGD/R group), liquiritigenin group (LIQ, 50 mM), inhibitor group (Bardoxolone, 10 mM), and liquiritigenin + inhibitor group (LIQ + Bardoxolone, 50 mM + 10 mM). After 24 h of intervention, the groups including the OGD/R group, liquiritigenin group, agonist group, and liquiritigenin + agonist group underwent oxygen-glucose deprivation/reoxygenation.

### **2.14. Annexin V-FITC and PI double staining method**

Start with a suspension of 50,000 to 100,000 cells and spin them down at 1000 g for 5 min. Carefully pour off the supernatant, then add 195  $\mu$ L of Annexin V-FITC binding solution to the pellet, gently resuspending the cells. Next, mix in 5  $\mu$ L of Annexin V-FITC, ensuring it's well combined. Add 10  $\mu$ L of propidium iodide staining solution and give it a gentle stir. Let the mixture sit in the dark at room temperature (20–25 °C) for 10 to 20 min, and then proceed with immediate flow cytometry analysis.

### **2.15. Detection of cell Nrf2/HO-1 signaling pathway expression**

After the culture medium was carefully aspirated from the 6-well plates, the cells underwent two thorough washes using ice-cold PBS buffer. Next, each well received 1 mL of PBS buffer, and the attached cells were delicately scraped off and transferred into microcentrifuge tubes that had been pre-cooled on ice. The cell suspension was spun down at 1200  $\times$  g for 5 min at 4 °C. After discarding the supernatant, the resulting cell pellet was gently resuspended in 150  $\mu$ L of ice-cold RIPA lysis buffer, which included 1% phenylmethylsulfonyl fluoride (PMSF). The mixture was then left on ice for half an hour, with thorough vortexing every 10 min to ensure optimal lysis. Once the three mixing intervals were complete, the lysate was centrifuged again at 15,000  $\times$  g for 15 min at 4 °C. The supernatant, now rich in total protein, was carefully divided into fresh microcentrifuge tubes and stored at –80 °C for future use.

Protein concentrations were determined using a BCA Protein Assay Kit (Pierce, USA) to ensure consistent loading amounts for SDS-PAGE. Equal protein amounts (20–30  $\mu$ g per lane) were separated on 10% SDS-PAGE gels under denaturing conditions and then transferred to PVDF membranes (Millipore, USA) at a steady current of 250 mA for one hour. To block non-specific interactions, the membranes were soaked in 5% non-fat milk dissolved in TBST (Tris-buffered saline with 0.1% Tween-20) for two hours at room temperature.

Next, the membranes were incubated with 5% skim milk for two hours at room temperature before being treated with primary antibodies (Nrf2, HO-1, Keap1) overnight at 4 °C. After three thorough washes with TBST, the membranes were exposed to HRP-conjugated secondary antibodies at 37 °C for one hour. Following another round of three washes with TBST and distilled water, protein bands were visualized using an ECL detection kit. The intensities of these bands were then analyzed using gel imaging software after exposure.

## 2.16. Statistical method

GraphPad Prism 9.0 (GraphPad Software, USA): Used for statistical calculations, graph generation, and dose-response modeling. SPSS 26.0 (IBM, USA): Applied for advanced multivariate analysis and data validation. ImageJ (NIH, USA): Utilized for quantitative analysis of Western blot bands, TUNEL-positive cell counts, and histopathological images.

The experimental results were presented as averages accompanied by their standard deviations ( $\pm$ SD). To evaluate variations across different groups, a one-way ANOVA was employed. For more detailed analysis, the Student-Newman-Keuls method was utilized to compare individual pairs. Statistical significance was determined at a threshold where the p-value fell below 0.05.

## 3. Results

### 3.1. LIQ improved cardiac function and hemodynamic parameters in MIRI rats

In contrast to the sham-operated group, rats in the MIRI model showed marked early arrhythmias and ST-segment elevation (**Figure 1C**). LIQ administration markedly reduced the ST-segment elevation and improved ventricular arrhythmias across all treatment groups.

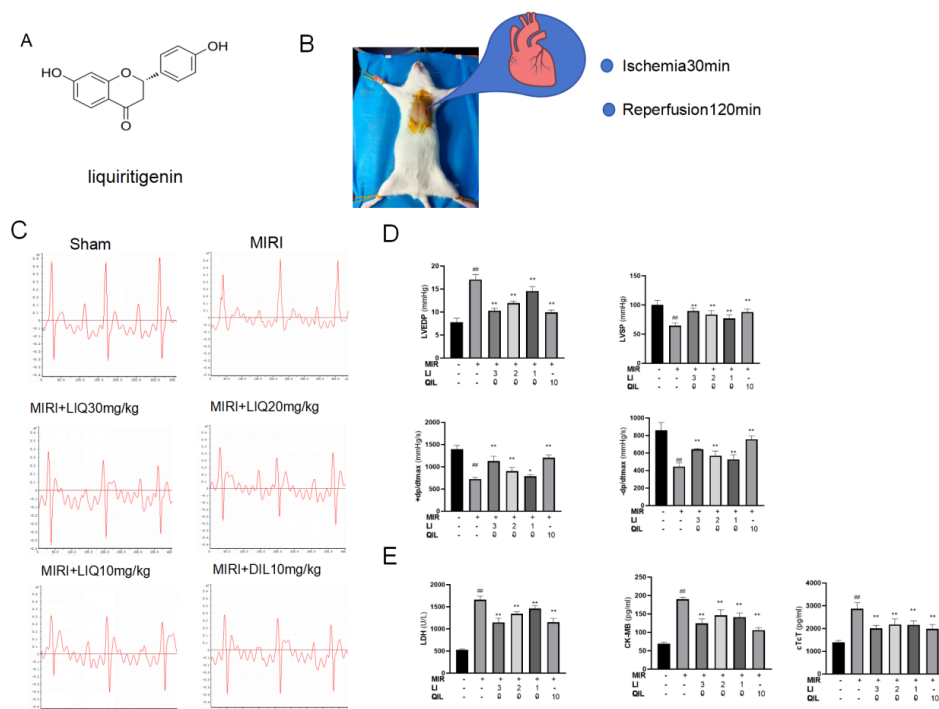


**Figure 1.** LIQ improved cardiac function and hemodynamic parameters in MIRI rats. **(A)** chemical structure of liquiritigenin; **(B)** MIRI model: 30-min ischemia followed by 120-min reperfusion; **(C)** ECG analysis showing; **(D)** hemodynamic parameters of left ventricular function. Left ventricular systolic pressure (LVSP). Left ventricular end-diastolic pressure (LVEDP). Maximum rates of left ventricular pressure rise (+dp/dtmax) and fall (-dp/dtmax). **(E)** Cardiac function index: LDH, CK-MB, and cTnT levels. Data are expressed as mean  $\pm$  SEM ( $n = 10$  per group).

Note: \*\* $p < 0.05$ , \*\*\* $p < 0.01$  vs. the MIRI group, ## $p < 0.05$  vs. the sham group.

Hemodynamic analysis indicated that, in contrast to the sham group ( $P < 0.01$ ), the MIRI group exhibited a marked decline in left ventricular systolic pressure (LVSP), as well as in the maximal rates of pressure rise/fall (+dp/dt<sub>max</sub>, -dp/dt<sub>max</sub>), and a notable increase in left ventricular end-diastolic pressure (LVEDP). This clearly pointed to severe cardiac impairment. Pretreatment with LIQ increased LVSP ( $P < 0.01$ ), reduced LVEDP ( $P < 0.01$ ), and restored +dp/dt<sup>max</sup>, -dp/dt<sup>max</sup> ( $P < 0.05$ ), demonstrating improved post-reperfusion cardiac pump function (**Figure 1D**).

### 3.2. LIQ attenuated myocardial oxidative stress injury

LDH and CK-MB serum levels were markedly higher in the MIRI group than in the sham group ( $P < 0.01$ ). LIQ intervention at high, medium, and low doses markedly reduced these levels ( $P < 0.01$ ) (**Figure 1E**).

Oxidative stress markers showed decreased myocardial SOD activity and GSH content ( $P < 0.01$ ), alongside increased MDA levels ( $P < 0.01$ ) in the MIRI group. LIQ pretreatment restored SOD activity and GSH content while reducing MDA levels ( $P < 0.01$ ), indicating suppression of reperfusion-induced oxidative stress (**Figure 2A**).

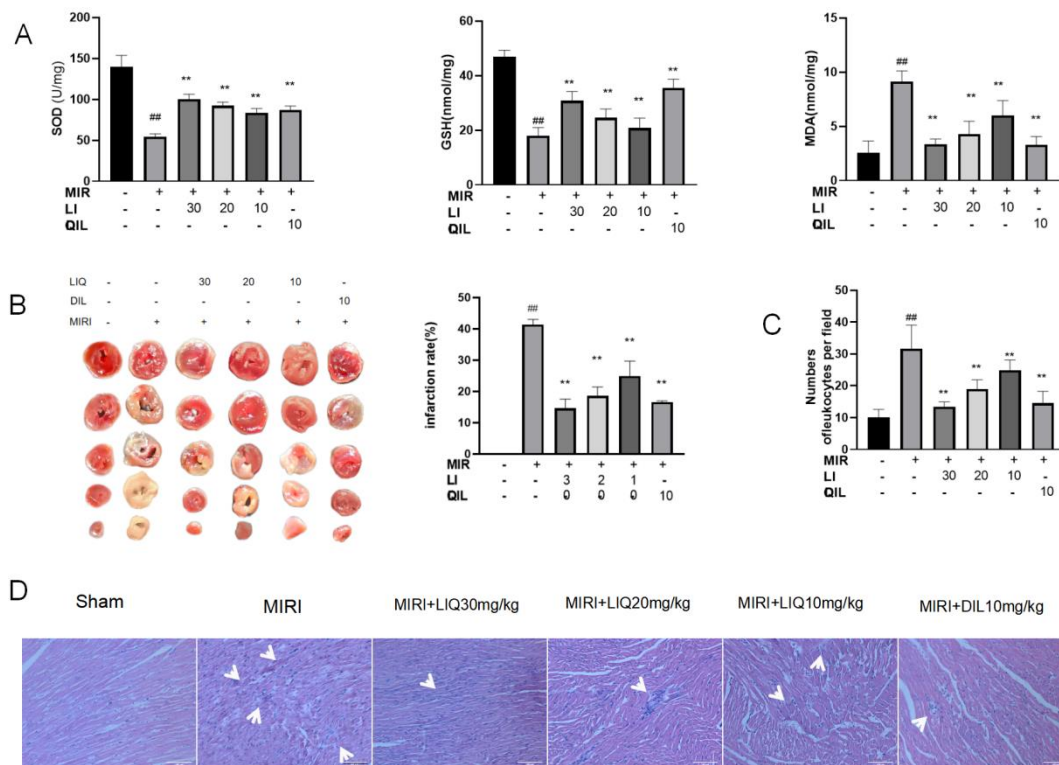


**Figure 2.** LIQ attenuated myocardial oxidative stress injury and the effect on pathology. **(A)** Oxidative stress index: SOD, GSH-Px, MDA levels. **(B)** Representative TTC stained heart sections and infarct size quantification. **(C)** Quantitative analysis of leukocyte infiltration in myocardial tissue. **(D)** Representative hematoxylin and eosin (HE) stained sections showing the I/R injury area myocardial tissue morphology. Data are expressed as mean  $\pm$  SEM ( $n = 10$  per group).

Note: \*  $p < 0.05$ , \*\*  $p < 0.01$  vs. the MIRI group, ##  $p < 0.05$  vs. the sham group.

### 3.3. LIQ reduced myocardial histopathological damage and apoptosis

TTC staining results (**Figure 2B**) showed that large-scale ischemia occurred in the heart tissue of rats in the model group, and the ischemic area was reduced after the

intervention of glycyrrhizin, especially in the high-dose group, the ischemic area was only 14.91% after quantization, which was much lower than that in the model group (39.93%) ( $P < 0.01$ ).

Histopathological evaluation (**Figure 2C,D**) revealed intact myocardial fibers and clear interstitial structures in the sham group. The MIRI group displayed characteristic ischemia-reperfusion injury, including myocardial fiber disruption, interstitial edema, and neutrophil/macrophage infiltration, with significantly elevated pathological scores ( $P < 0.01$  vs. sham). LIQ exerted dose-dependent protection: the medium-dose group (20 mg/kg) reduced injury scores, while the high-dose group (30 mg/kg) achieved further improvement ( $P < 0.001$ ), comparable to the positive control. TUNEL assays (**Figure 3A**) showed a significantly increased apoptosis index in the MIRI group ( $P < 0.01$  vs. sham). LIQ intervention reduced apoptosis indices across all dose groups ( $P < 0.01$ ).

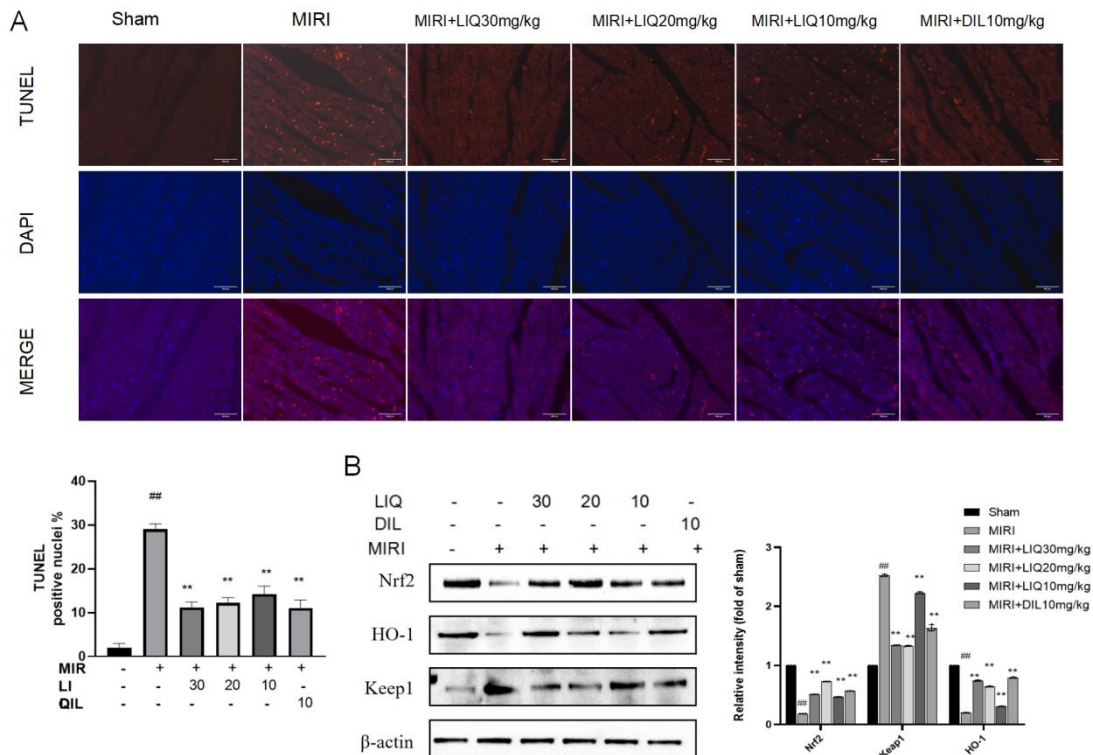


**Figure 3.** Liquiritigenin attenuates myocardial apoptosis in rat models by modulating the Nrf2/HO-1 signaling pathway. **(A)** Representative TUNEL staining images showing apoptotic cells (red) and nuclei (blue). Quantitative analysis of apoptotic index. **(B)** Protein expressions of Nrf2, HO-1, Keap1, and β-actin were used as an internal control for sample loading. Data are expressed as mean ± SEM ( $n = 3$  per group).

Note: \*  $p < 0.05$ , \*\*  $p < 0.01$  vs. the MIRI group, ##  $p < 0.05$  vs. the sham group.

### 3.4. LIQ stimulated the Nrf2/HO-1 pathway

Western blot analysis revealed a marked reduction in myocardial Nrf2 protein expression in the myocardial ischemia-reperfusion injury (MIRI) group, with statistical significance ( $P < 0.01$ ). This finding underscores the impairment of the Nrf2 signaling pathway under ischemic conditions. Notably, pretreatment with LIQ (liquiritigenin) exerted a significant inhibitory effect on Keap1 protein degradation ( $P < 0.01$ ), suggesting its role in stabilizing this negative regulator of Nrf2. Furthermore,

LIQ treatment was associated with a substantial upregulation of heme oxygenase-1 (HO-1) expression ( $P < 0.01$ ), indicating its potential to enhance antioxidant defenses. Comparative analysis demonstrated that LIQ pretreatment not only restored Nrf2 levels but also significantly elevated HO-1 expression relative to the MIRI group, while concurrently reducing Keap1 expression. These results, as illustrated in **Figure 3B**, collectively highlight the therapeutic potential of LIQ in modulating the Nrf2-Keap1-HO-1 signaling axis to mitigate oxidative stress and cellular damage in myocardial ischemia-reperfusion injury.

### 3.5. Liquiritigenin reduces OGD/R-induced apoptosis in H9C2 cells

The process of apoptosis in H9C2 cells was assessed through flow cytometry analysis. OGD/R significantly triggered cellular apoptosis, with both early and late apoptosis rates markedly increased in the OGD/R group, and the total apoptosis rate was substantially higher than that in the control group ( $P < 0.01$ ). Intervention with LIQ or an Nrf2 agonist significantly attenuated OGD/R-induced cardiomyocyte apoptosis ( $P < 0.01$ ). Notably, in late apoptosis, the rates decreased to 9.45% and 12.68% in the LIQ intervention group and Nrf2 agonist group, respectively, indicating that LIQ and the Nrf2 agonist effectively inhibited cardiomyocyte apoptosis triggered by OGD/R, thereby exerting cardioprotective effects. Notably, the LIQ group, Nrf2 agonist group, and LIQ + Nrf2 agonist group demonstrated comparable reductions in apoptosis, suggesting that LIQ reduces cardiomyocyte apoptosis and safeguards myocardial tissue mainly via Nrf2 pathway activation (**Figure 4A**).

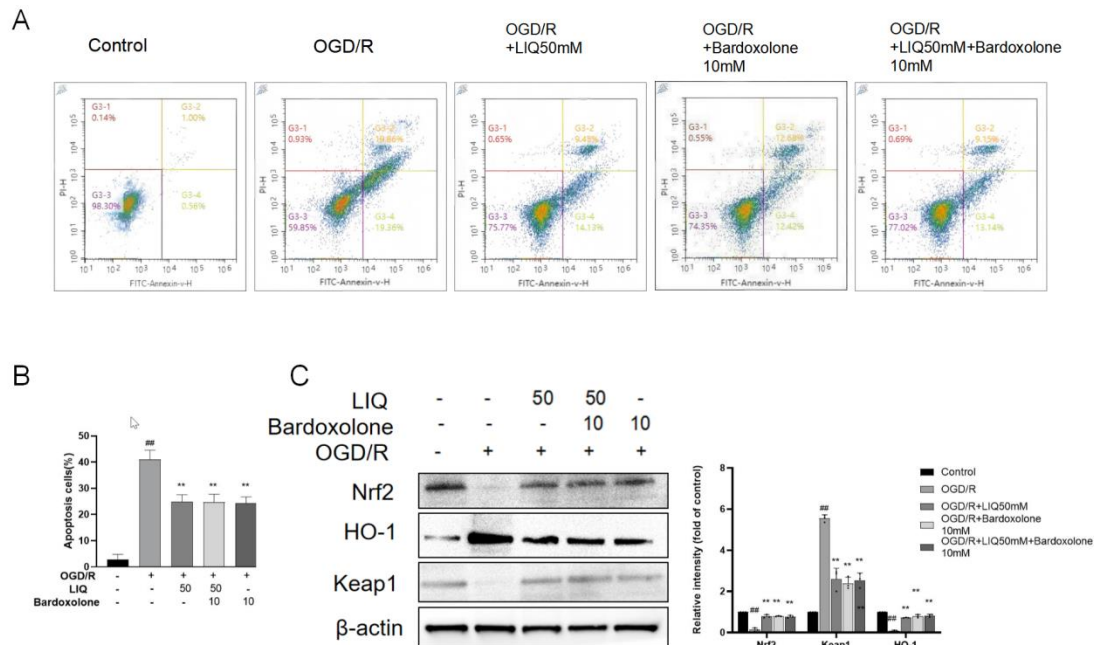


**Figure 4.** Liquiritigenin attenuates OGD/R model H9C2 cells by modulating the Nrf2/HO-1 signaling pathway. **(A)** Apoptosis was detected by flow cytometry. The apoptotic rates were presented as the sum of the percentages of cells in the early apoptotic phase and late apoptotic phase. **(B)** Quantitative analysis of apoptotic index. **(C)** Protein expressions of Nrf2, HO-1, Keap1, and  $\beta$ -actin were used as an internal control for sample loading. Data are expressed as mean  $\pm$  SEM ( $n = 3$  per group).

Note: \*  $p < 0.05$ , \*\*  $p < 0.01$  vs. the MIRI group, ##  $p < 0.05$  vs. the sham group.

### 3.6. LIQ activates the Nrf2/HO-1 signaling pathway in H9C2 cells

Mirroring observations from live animal studies, lab-based experiments demonstrated that oxygen-glucose deprivation followed by reoxygenation (OGD/R) led to a marked decrease in Nrf2 and HO-1 protein expression in H9C2 cells. Simultaneously, Keap1 levels surged, suggesting that heightened oxidative stress after hypoxia-reoxygenation plays a pivotal role in dampening the Nrf2/HO-1 signaling pathway. These findings underscore the intricate link between oxidative damage and the suppression of this critical cellular defense mechanism. Following treatment with liquiritigenin (LIQ) or an Nrf2 agonist, the expression of Nrf2 and HO-1 proteins was markedly upregulated compared to the OGD/R group, accompanied by reduced Keap1 levels. Notably, the LIQ group, Nrf2 agonist group, and LIQ + Nrf2 agonist group showed no significant differences in these effects, demonstrating that LIQ protects H9C2 cells by triggering the Nrf2/HO-1 pathway to reduce oxidative stress after hypoxia-reoxygenation. The results of the Western blot analysis revealed a notable decline in myocardial Nrf2 protein levels within the MIRI group, with statistical significance ( $P < 0.01$ ). Interestingly, LIQ treatment effectively curbed the degradation of Keap1 protein ( $P < 0.01$ ) and boosted the expression of HO-1 ( $P < 0.01$ ). When compared to the MIRI group, pretreatment with LIQ led to a marked increase in both Nrf2 and HO-1 levels while simultaneously lowering Keap1 expression, as illustrated in **Figure 3B**.

## 4. Discussion

This study introduced a MIRI model using an adjusted approach to occlude the left anterior descending coronary artery. Through a thoracotomy, a reversible ligature was placed approximately 2–3 mm beyond the artery's origin, maintaining occlusion for 30 min, followed by a 120-min reperfusion period. This standardized modeling approach is based on the anatomical characteristics of the LAD as the primary blood supply to the left ventricle. Its occlusion effectively simulates clinical acute myocardial ischemic events, while timely reperfusion accurately replicates the re-injury process post-revascularization therapy [7]. Notably, the model parameters (30 min ischemia/120 min reperfusion) were validated in our prior systematic studies [8], ensuring injury severity that mimics common clinical ischemic timeframes while avoiding irreversible myocardial necrosis, thereby demonstrating excellent controllability and reproducibility.

The results revealed that the experimental rats exhibited typical acute myocardial injury characteristics. Lead II ECG revealed ST elevation with convex curvature and inverted T waves, indicative of STEMI [9]. Hemodynamic analysis showed reduced LVSP and elevated LVEDP in the model group. Histopathological examination demonstrated disorganized myocardial cell arrangement, blurred striations, interstitial edema, and significant inflammatory infiltration in the ligated area. These multi-dimensional outcomes align with internationally recognized Langendorff model evaluation criteria and our previously established injury assessment system [8], confirming successful model replication. The stable animal model provides a reliable experimental platform, with reproducible pathophysiological processes ensuring scientific validity and comparability of data, thereby laying a solid foundation for

exploring MIRI mechanisms.

Compared to the model group, liquiritigenin (LIQ) pretreatment effectively alleviated ventricular arrhythmias in MIRI rats, significantly reduced ST-segment elevation, and improved hemodynamic function (increased LVSP, +dp/dtmax, and -dp/dtmax; decreased LVEDP). LIQ also slowed myocardial cell injury progression (improved HE histopathology) in a dose-dependent manner. Furthermore, LIQ enhanced antioxidant capacity (elevated SOD activity, increased GSH levels, reduced MDA content) and reduced myocardial apoptosis (TUNEL assay). As a result, LIQ effectively mitigates cardiac injury caused by MIRI by curbing oxidative stress and preventing cell death.

The Nrf2/HO-1 signaling pathway plays a critical role in the progression of MIRI, as it directly impacts oxidative stress, inflammatory responses, and the apoptosis of myocardial cells [10]. The Nrf2 protein, weighing 66 kDa, features a conserved bZIP domain and seven homologous regions (Neh1-7). The Neh1 region contains the bZIP structural element, which binds to the transcriptional partner sMaf to form a dimer essential for DNA binding and transcriptional activation. The Neh2 region features dual interaction sites: DLG and ETGE. These motifs primarily interact with the DGR domain of Keap1, Nrf2's negative regulator, to mediate its ubiquitination and degradation under basal conditions [11]. To counteract diverse stressors, Keap1 employs multiple mechanisms to activate Nrf2. A canonical molecular model for Nrf2 activation is the "hinge-latch mechanism": Under normal biological states, Keap1 interacts with the DLG region of Nrf2, facilitating its ubiquitination and proteasomal degradation. During oxidative stress, the DLG motif dissociates from Keap1, and the ETGE motif functions as a "hinge", sustaining partial binding. This conformational change stabilizes Nrf2 by preventing degradation and promotes its nuclear translocation [12].

Nrf2's primary physiological role is to regulate cellular antioxidant responses. Normally, cytosolic Nrf2 forms a complex with Keap1 and exhibits an extremely short half-life (10–30 min), undergoing rapid ubiquitination and proteasomal degradation [12]. Under oxidative stress, inflammation, or metabolic stress [13], Keap1 experiences structural alterations, facilitating the release of Nrf2 for nuclear translocation. Nrf2 dimerizes with sMaf in the nucleus, and this heterodimer binds to antioxidant response elements (ARE) within target gene promoters. This process kicks off the activation of various antioxidant and detoxification enzymes, including NAD(P)H quinone oxidoreductase 1 (NQO1), superoxide dismutase (SOD), glutathione peroxidase (GSH-Px), catalase (CAT), and heme oxygenase-1 (HO-1). Essentially, it sets the stage for the body's defense mechanisms to ramp up, helping to neutralize harmful substances and oxidative stress.

Nrf2 exerts its antioxidative effects through two key mechanisms: Classical antioxidant enzyme regulation: Upregulating SOD, CAT, and GSH-Px expression to neutralize reactive oxygen species (ROS). Redox homeostasis modulation: Enhancing glutathione (GSH) biosynthesis. Increasing HO-1 and NQO1 protein expression to degrade pro-oxidant heme and xenobiotics. These coordinated actions maintain cellular redox balance and protect against oxidative damage.

Nrf2, a key regulator of redox homeostasis, binds to antioxidant response elements (ARE) via its Neh1 domain, stimulating antioxidant enzyme production (e.g.,

SOD, CAT) to boost ROS elimination and mitigate oxidative stress [14,15]. This mechanism is pivotal in cardiac protection [16]. Studies highlight Nrf2's essential role in mitigating MIRI [17]. HO-1 (molecular weight ~32 kDa), a rate-limiting enzyme in heme degradation [18], exerts dual cytoprotective effects: (1) degrading heme to neutralize excess superoxide and ROS from heme-containing oxidases, and (2) generating antioxidative and antiapoptotic products (carbon monoxide, ferrous iron, biliverdin) during heme catabolism [19–21]. Nrf2-ARE binding activates HO-1 expression, which boosts the function of phase II antioxidant enzymes (SOD, CAT, GSH-Px). Bellezza et al. [22] effectively eliminating free radicals and reducing oxidative injury. Both in MIRI rat and in OGD/R H9C2 cells, studies confirm that the Nrf2/HO-1 pathway alleviates MIRI. For instance, baicalin and wogonoside attenuate apoptosis, inflammation, and fibrosis in MIRI by modulating this pathway [23], while Nrf2/HO-1 activation mitigates myocardial damage in murine MIRI models via endoplasmic reticulum stress amelioration [24]. Consistent with prior findings, our study demonstrated decreased Nrf2 and HO-1 protein expression, elevated Keap1 levels, intensified oxidative stress (increased MDA, reduced SOD/GSH), and enhanced myocardial apoptosis in MIRI rats. LIQ pretreatment reversed these effects, enhancing Nrf2/HO-1, inhibiting Keap1, and decreasing oxidative stress and apoptosis.

## 5. Conclusion

This research presents the initial proof that Liquiritigenin alleviates MIRI-induced cardiac impairment. It does so by triggering the Nrf2/HO-1 signaling pathway, which in turn curbs oxidative stress and apoptosis. These findings offer theoretical support for developing natural product-based cardioprotective agents and underscore the therapeutic potential of targeting antioxidant pathways in cardiovascular diseases.

**Author contributions:** Conceptualization, HJ and SL; methodology, TW; software, MS; data curation, ZM; writing—original draft preparation, HJ; funding acquisition, HJ and SL. All authors have read and agreed to the published version of the manuscript.

**Funding:** This research was funded by Anhui Province's health initiative (NO. AHWJ2022b007) and Anhui university research project (NO. 2024AH050858).

**Ethical approval:** The study was conducted in accordance with the Declaration of Helsinki, and approved by the Ethics Committee of Anhui Academy of Medical Sciences (Permit No. 2022 - LLBG - 017). Every possible measure was taken to guarantee that all experimental animals were treated ethically and that their suffering was kept to a minimum.

**Conflict of interest:** The authors declare no conflict of interest.

## References

1. Zeng C, Jiang W, Zheng R, et al. Cardioprotection of tilianin ameliorates myocardial ischemia-reperfusion injury: Role of the apoptotic signaling pathway. Fan GC, ed. PLOS ONE. 2018; 13(3): e0193845. doi: 10.1371/journal.pone.0193845
2. Zhang XJ, Liu X, Hu M, et al. Pharmacological inhibition of arachidonate 12-lipoxygenase ameliorates myocardial

- ischemia-reperfusion injury in multiple species. *Cell Metabolism*. 2021; 33(10): 2059-2075.e10. doi: 10.1016/j.cmet.2021.08.014
3. Yang Z, Xie Y, Li M, et al. Ramelteon alleviates myocardial ischemia/reperfusion injury (MIRI) through Sirt3-dependent regulation of cardiomyocyte apoptosis. *Biomedicine & Pharmacotherapy*. 2024; 172: 116229. doi: 10.1016/j.biopha.2024.116229
  4. Valikeserlis I, Athanasiou AA, Stakos D. Cellular mechanisms and pathways in myocardial reperfusion injury. *Coronary Artery Disease*. 2021; 32(6): 567-577. doi: 10.1097/mca.0000000000000997
  5. Yao D, Bao L, Wang S, et al. Isoliquiritigenin alleviates myocardial ischemia-reperfusion injury by regulating the Nrf2/HO-1/SLC7a11/GPX4 axis in mice. *Free Radical Biology and Medicine*. 2024; 221: 1-12. doi: 10.1016/j.freeradbiomed.2024.05.012
  6. Li L, Fang H, Yu YH, et al. Liquiritigenin attenuates isoprenaline-induced myocardial fibrosis in mice through the TGF- $\beta$ 1/Smad2 and AKT/ERK signaling pathways. *Molecular Medicine Reports*. 2021; 24(4). doi: 10.3892/mmr.2021.12326
  7. Tong HQ, Fan ML, Sun T, et al. Improved Rodent Model of Myocardial Ischemia and Reperfusion Injury. *Journal of Visualized Experiments*. 2022; (181). doi: 10.3791/63510-v
  8. Luo SY, Chen S, Qin YD, et al. Urotensin-II Receptor Antagonist SB-710411 Protects Rat Heart against Ischemia-Reperfusion Injury via RhoA/ROCK Pathway. Gallyas F, ed. *PLOS ONE*. 2016; 11(1): e0146094. doi: 10.1371/journal.pone.0146094
  9. Xu K, Yang Y, Lan M, et al. Apigenin alleviates oxidative stress-induced myocardial injury by regulating SIRT1 signaling pathway. *European Journal of Pharmacology*. 2023; 944: 175584. doi: 10.1016/j.ejphar.2023.175584
  10. Zhong Z, Luo XY, Xiang P, et al. MRTF-A alleviates myocardial ischemia reperfusion injury by inhibiting the inflammatory response and inducing autophagy. *Molecular and Cellular Biochemistry*. 2022; 478(2): 343-359. doi: 10.1007/s11010-022-04510-4
  11. Hayes JD, Dinkova-Kostova AT. The Nrf2 regulatory network provides an interface between redox and intermediary metabolism. *Trends in Biochemical Sciences*. 2014; 39(4): 199-218. doi: 10.1016/j.tibs.2014.02.002
  12. Kobayashi M, Yamamoto M. Nrf2-Keap1 regulation of cellular defense mechanisms against electrophiles and reactive oxygen species. *Advances in Enzyme Regulation*. 2006; 46(1): 113-140. doi: 10.1016/j.advenzreg.2006.01.007
  13. Dodson M, de la Vega MR, Cholanians AB, et al. Modulating NRF2 in Disease: Timing Is Everything. *Annual Review of Pharmacology and Toxicology*. 2019; 59(1): 555-575. doi: 10.1146/annurev-pharmtox-010818-021856
  14. Egbujor MC, Buttari B, Profumo E, et al. An Overview of NRF2-Activating Compounds Bearing  $\alpha,\beta$ -Unsaturated Moiety and Their Antioxidant Effects. *International Journal of Molecular Sciences*. 2022; 23(15): 8466. doi: 10.3390/ijms23158466
  15. Zhang W, Feng C, Jiang H. Novel target for treating Alzheimer's Diseases: Crosstalk between the Nrf2 pathway and autophagy. *Ageing Research Reviews*. 2021; 65: 101207. doi: 10.1016/j.arr.2020.101207
  16. Wang R, Wu Y, Jiang S. FOXC2 Alleviates Myocardial Ischemia-Reperfusion Injury in Rats through Regulating Nrf2/HO-1 Signaling Pathway. Pichini S, ed. *Disease Markers*. 2021; 2021: 1-9. doi: 10.1155/2021/9628521
  17. Lu P, Qi Y, Li X, et al. PEDF and 34-mer peptide inhibit cardiac microvascular endothelial cell ferroptosis via Nrf2/HO-1 signalling in myocardial ischemia-reperfusion injury. *Journal of Cellular and Molecular Medicine*. 2024; 28(14). doi: 10.1111/jcmm.18558
  18. Choi AM, Alam J. Heme oxygenase-1: function, regulation, and implication of a novel stress-inducible protein in oxidant-induced lung injury. *American Journal of Respiratory Cell and Molecular Biology*. 1996; 15(1): 9-19. doi: 10.1165/ajrcmb.15.1.8679227
  19. Qiu Y, Wu Y, Meng M, et al. GYY4137 protects against myocardial ischemia/reperfusion injury via activation of the PHLPP-1/Akt/Nrf2 signaling pathway in diabetic mice. *Journal of Surgical Research*. 2018; 225: 29-39. doi: 10.1016/j.jss.2017.12.030
  20. Luo W, Li J, Li Z, et al. HO-1 nuclear accumulation and interaction with NPM1 protect against stress-induced endothelial senescence independent of its enzymatic activity. *Cell Death & Disease*. 2021; 12(8). doi: 10.1038/s41419-021-04035-6
  21. Sohn E, Kim YJ, Kim JH, et al. Ficus erecta Thunb Leaves Alleviate Memory Loss Induced by Scopolamine in Mice via Regulation of Oxidative Stress and Cholinergic System. *Molecular Neurobiology*. 2021; 58(8): 3665-3676. doi: 10.1007/s12035-021-02358-1
  22. Bellezza I, Giambanco I, Minelli A, et al. Nrf2-Keap1 signaling in oxidative and reductive stress. *Biochimica et Biophysica*

- Acta (BBA) - Molecular Cell Research. 2018; 1865(5): 721-733. doi: 10.1016/j.bbamcr.2018.02.010
23. Zhang B, Xu D. Wogonoside preserves against ischemia/reperfusion-induced myocardial injury by suppression of apoptosis, inflammation, and fibrosis via modulating Nrf2/HO-1 pathway. *Immunopharmacology and Immunotoxicology*. 2022; 44(6): 877-885. doi: 10.1080/08923973.2022.2090955
  24. Wang J, Lu L, Chen S, et al. Up-regulation of PERK/Nrf2/HO-1 axis protects myocardial tissues of mice from damage triggered by ischemia-reperfusion through ameliorating endoplasmic reticulum stress. *Cardiovascular Diagnosis and Therapy*. 2020; 10(3): 500-511. doi: 10.21037/cdt-20-126